Development/Plasticity/Repair

The Distinct Temporal Origins of Olfactory Bulb Interneuron Subtypes

Renata Batista-Brito,[1,2,4]* Jennie Close,[1,2]* Robert Machold,[1,3] and Gord Fishell[1,2]

[1]Smilow Neuroscience Program and Departments of [2]Cell Biology and [3]Otolaryngology, New York University Medical Center, New York, New York 10016, and [4]Gulbenkian PhD Programme in Biomedicine, Gulbenkian Science Institute, 2781-901 Oeiras, Portugal

Olfactory bulb (OB) interneurons are a heterogeneous population produced beginning in embryogenesis and continuing through adulthood. Understanding how this diversity arises will provide insight into how OB microcircuitry is established as well as adult neurogenesis. Particular spatial domains have been shown to contribute specific interneuron subtypes. However, the temporal profile by which OB interneuron subtypes are produced is unknown. Using inducible genetic fate mapping of *Dlx1/2* precursors, we analyzed the production of seven OB interneuron subtypes and found that the generation of each subpopulation has a unique temporal signature. Within the glomerular layer, the production of tyrosine hydroxylase-positive interneurons is maximal during early embryogenesis and decreases thereafter. In contrast, the generation of calbindin interneurons is maximal during late embryogenesis and declines postnatally, whereas calretinin (CR) cell production is low during embryogenesis and increases postnatally. Parvalbumin interneurons within the external plexiform layer are produced only perinatally, whereas the generation of 5T4-positive granule cells in the mitral cell layer does not change significantly over time. CR-positive granule cells are not produced at early embryonic time points, but constitute a large percentage of the granule cells born after birth. Blanes cells in contrast are produced in greatest number during embryogenesis. Together we provide the first comprehensive analysis of the temporal generation of OB interneuron subtypes and demonstrate that the timing by which these populations are produced is tightly orchestrated.

Key words: **genetic fate mapping; adult stem cells; neuronal birthdate; interneurons; neurogenesis; olfactory bulb**

Introduction

Odor information is relayed by sensory neurons to the olfactory bulb (OB), where it is processed by complex local microcircuitry (Firestein, 2001). This is mediated largely through the actions of a diverse set of interneurons (Aungst et al., 2003; Lledo et al., 2005). Subpopulations of these interneurons can be characterized by their location, synaptic connectivity, morphology, firing patterns, and expression of a variety of immunomarkers (Price and Powell, 1970a,c; Pinching and Powell, 1971a; Shipley and Ennis, 1996; Crespo et al., 2001; McQuiston and Katz, 2001; Kosaka and Kosaka, 2005).

Numerous studies have demonstrated that OB interneurons are derived from molecularly defined, spatially distinct progenitor regions. Namely, embryonically derived OB interneurons have been shown to arise from the lateral ganglionic eminence (LGE) and dorsal telencephalon (Toresson and Campbell, 2001; Wichterle et al., 2001; Gorski et al., 2002; Willaime-Morawek et al., 2006; Kohwi et al., 2007; Ventura and Goldman, 2007), whereas postnatally they are derived from the subventricular zone (SVZ) of the lateral ventricle (Doetsch et al., 1997, 1999; Luskin, 1998; Alvarez-Buylla and Garcia-Verdugo, 2002). Within these general progenitor domains, it has recently been demonstrated that specific subtypes arise from spatially defined progenitor populations (Merkle et al., 2007).

The temporal aspects of OB interneuron generation are of particular interest, because thymidine analog birthdating has shown that OB interneuron production begins embryonically and continues throughout the life of the animal (Hinds, 1968a,b; Bayer, 1983). Although these studies have provided valuable information regarding the numbers and timing of OB cell production, they have not investigated interneuron subtype production over time. In an attempt to determine the temporal specificity of glomerular layer interneuron production, a recent study has used *in situ* dye labeling and OB progenitor transplants to address the issue (De Marchis et al., 2007). However, in light of the recently discovered importance of spatial origin of OB progenitors, these methods might be subject to bias depending on the location of dye injection, source of transplanted progenitors, or differential survival of progenitor subtypes upon transplantation. Furthermore, no study has investigated the temporal production of subglomerular layer OB interneuron subtypes.

Received Dec. 19, 2007; revised Jan. 25, 2008; accepted Feb. 17, 2008.

This work was supported by National Institutes of Health Grants R01MH068469 from the National Institute of Mental Health, R01NS039007 from the National Institute of Neurological Disorders and Stroke (both to G.F.), and 5F32DC008262 from the National Institute on Deafness and Other Communication Disorders (J.C.), and by the Science and Technology Foundation of Portugal Grant (R.B.-B.). We thank Noël Ghanem and Mark Ekker (University of Ottawa, Ottawa, Ontario, Canada) for the Dlx1/2 enhancer, Ken Bainbridge (University of British Columbia, Vancouver, British Columbia, Canada) for the parvalbumin antibody, and Kensaku Mori (University of Tokyo, Tokyo, Japan) for the 5T4 antibody. We also thank Lihong Yin and Jiali Deng for technical assistance.

*R.B.-B. and J.C. contributed equally to this work.

Correspondence should be addressed to Gord Fishell, Smilow Neuroscience Program and the Department of Cell Biology, Smilow Research Building, New York University Medical Center, 522 First Avenue, New York, NY 10016. E-mail: fishell@saturn.med.nyu.edu.

DOI:10.1523/JNEUROSCI.5625-07.2008

 0270-6474/08/283966-10$15.00/0

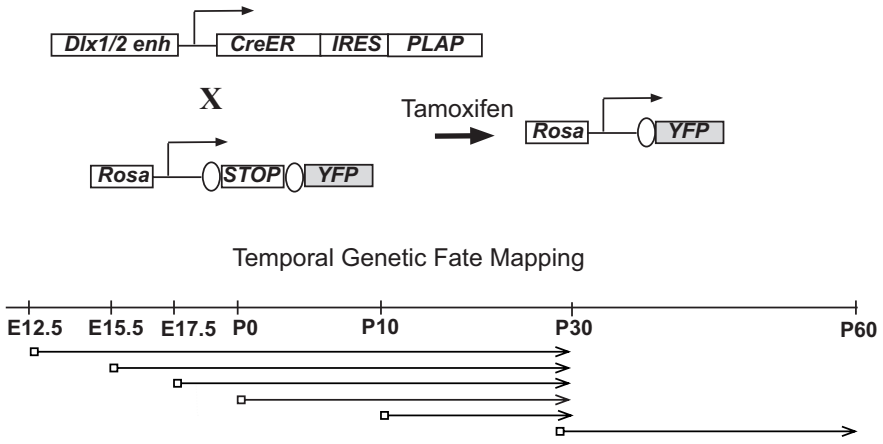

Figure 1. Fate-mapping strategy of OB interneuron progenitors. Mice expressing tamoxifen-inducible CreER under the control *Dlx1/2* intragenic enhancer region, crossed with the *RosaYFP* reporter line, which express YFP after LoxP recombination. Tamoxifen was administered at the indicated time points, and the OBs were analyzed at P30 and P60.

To systematically explore the temporal origins of OB interneurons, we have performed inducible genetic fate mapping of OB interneuron precursors using a *Dlx1/2-CreER* transgenic line, which labels OB interneurons in every layer of the olfactory bulb. This transgene allows us to temporally label OB interneuron precursors from embryogenesis through adulthood and follow their fate *in vivo* in a noninvasive, temporally specific manner. We find that the proportion of cells destined for the glomerular layer (GL) decreases with the age of the animal, with a concomitant increase in the proportion of labeled cells destined for the granule cell layer (GCL). In addition to tyrosine hydroxylase (TH)-, calbindin (CB)-, and calretinin (CR)-positive GL subtypes, we also describe the production of parvalbumin-positive (PV+) cells of the external plexiform layer (EPL), 5T4- and CR-positive granule cell subpopulations, and Blanes cells. We demonstrate that each OB interneuron subtype derived from the *Dlx1/2* lineage has a unique temporal pattern of production.

Materials and Methods

DLX1/2-CreER *transgene construction.* The *Dlx1/2* intergenic enhancer I12b (Ghanem et al., 2007) cDNA was subcloned into the 3′ end of an expression construct consisting of a thymidine kinase minimal promoter upstream of a cDNA encoding the T2 mutant form of a Cre recombinase–estrogen receptor fusion (Feil et al., 1997), followed by an IRES (internal ribosomal entry site) sequence and the cDNA for human placental alkaline phosphatase (PLAP), followed by three SV40 poly A tandem repeats. Transgenic mice were generated as previously described (Nagy et al., 2003). Nine founder lines were obtained, and one line was selected for further studies based on both its high fidelity of expression compared with that directed from the endogenous locus (as determined by PLAP histochemistry) and its efficiency in mediating tamoxifen-dependent cell labeling of the R26R reporter line (Zambrowicz et al., 1997; Srinivas et al., 2001).

Animals. Dlx1/2-CreER transgenic, *RosaYFP* heterozygous (Srinivas et al., 2001) males were crossed to 7- to 8-week-old wild-type Swiss Webster females (Taconic, Germantown, NY). Four milligrams of tamoxifen solution (Sigma, St. Louis, MO) at 20 mg/ml in corn oil (Sigma) were given to pregnant mothers by oral gavaging at embryonic day 12.5 (E12.5), E15.5, and E17.5. After birth, 1 mg [postnatal day 0 (P0)], 2 mg (P10), or 4 mg (P30) of tamoxifen solution was given by intraperitoneal injection. PCR genotyping of *Dlx1/2-CreER* transgene and *Rosa*YFP allele were performed by using the primers specific to *Cre* [forward (F), taaagatatctcacgtactgacggtg; reverse (R), tctctgaccagagtcatccttagc] and *YFP* (F, acaccctggtgaaccgcatcgag; R, gcgcttctcgttggggtctttgc).

Immunohistochemistry. Short-term fate mapping was analyzed by YFP expression 24 h after tamoxifen administration. Brains were fixed by transcardiac perfusion followed by 30 min of postfixation on ice with 4% paraformaldehyde/PBS solution. Brains were rinsed with PBS and cryoprotected by using a 30% sucrose/PBS solution overnight at 4°C. Olfactory bulb cryosections (20 μm) were obtained at P30 and P60. A minimum of four brains were analyzed for each time point. Blocking steps were performed by PBS solution containing 2% normal goat serum and 0.1% Triton X-100, followed by primary antibody incubation in 0.1% Triton X-100/PBS overnight at 4°C, four 5 min PBS rinses, and 1 h of secondary antibody incubation at room temperature in 0.1% Triton X-100/PBS, followed by four 5 min PBS rinses. Nuclear counterstaining was performed with 100 ng/ml 4′,6-diamidino-2-phenylindole (DAPI) solution in water for 5 min. Antibodies were used in the following concentrations: rat anti-platelet-derived growth factor receptor (PDGFR; 1:500; BD PharMingen, San Diego, CA), rabbit anti-GFP (1:1000; Invitrogen, Carlsbad, CA), rat anti-GFP (1:1000; Nacalai Tesque, Kyoto, Japan), mouse anti-GFAP (1:400; Millipore Bioscience Research Reagents, Temecula, CA), guinea pig anti-PV (1:1000), mouse anti-CR (1:1500; Millipore Bioscience Research Reagents), mouse anti-CB (1:1000; Sigma C-9848), rabbit anti-TH (1:500; Millipore Bioscience Research Reagents), rabbit anti 5T4 (1:2000; gift from Dr. Kensaku Mori, University of Tokyo, Tokyo, Japan), rabbit anti-cleaved caspase-3 (1:300; Cell Signaling, Danvers, MA). Fluorescent images for cell counting were captured using a cooled CCD camera (Princeton Scientific Instruments, Trenton, NJ) using MetaMorph software (Universal Imaging, Downingtown, PA). Confocal images were taken using a Zeiss (Thornwood, NY) LSM 510 META confocal microscope.

In situ *hybridization.* mRNA *in situ* hybridizations were performed as described previously (Wilkinson and Nieto, 1993). RNA probes were labeled with digoxigenin and visualized with BM-Purple, according to the manufacturer's instructions (Roche Biosciences, Palo Alto, CA). The cRNA probes used included *Dlx2* (Bulfone et al., 1993) and *CreER*. Images were obtained by bright-field photography on a Zeiss Axioscope using Spot Advanced software.

Results

Inducible genetic fate mapping of *Dlx1/2* precursors

Previous studies have shown that OB interneuron precursors derive from multiple locations, including the LGE, SVZ, septum, pallium, and rostral migratory stream (RMS) (Luskin and Boone, 1994; Wichterle et al., 2001; Stenman et al., 2003; Hack et al., 2005; Kohwi et al., 2007; Merkle et al., 2007; Ventura and Goldman, 2007). Despite their varied sites of origin, most, if not all, OB interneuron (GABAergic and dopaminergic) precursors require the expression of *Dlx1* and/or *Dlx2* for their generation, as evidenced by the virtual absence of GABAergic and dopaminergic OB interneurons in *Dlx1/Dlx2* null compound mutants (Anderson et al., 1997; Bulfone et al., 1998; Long et al., 2007). Thus, to genetically identify the temporal origins of OB interneurons, we fate mapped *Dlx1/2*-expressing precursors at different time points. To achieve this, we took advantage of two genetically modified alleles: a driver transgenic line *Dlx1/2-CreER*, expressing CreER under the control of *Dlx1/2* intragenic enhancer, and the *RosaYFP* reporter line (Srinivas et al., 2001), which expresses YFP after tamoxifen-induced Cre-mediated recombination of the stop cassette (Fig. 1). The intragenic enhancer used, I12b, has been previously shown to be broadly expressed in all the *Dlx1/2* precursor domains by analysis of lacZ expression of *I12b-lacZ* transgenic embryos (Ghanem et al., 2007). Furthermore, this

pan-interneuron transgenic line labels all the known mature interneuron subtypes (Ghanem et al., 2007), indicating that CreER under the control of this element should be initiated in all *Dlx1/2*-expressing precursor cells.

It has been previously reported that OB interneurons start to be born at E14.5 and continue to be born throughout life (Bayer, 1983; Luskin, 1993; Tucker et al., 2006). We fate mapped OB interneuron precursors expressing Dlx1/2 by transiently activating *Dlx1/2-CreER* by tamoxifen administration at the following ages: E12.5, E15.5, E17.5, P0, P10, and P30, followed by immunohistochemical analysis of the different subtypes at P30 and/or P60 (Fig. 1).

Short-term fate mapping of Dlx1/2 progenitors

Analysis of the *Dlx1/2-CreER* transgenic line was performed by comparing *Dlx2* and *CreER* expression (Fig. 2*A*,*B*,*D*,*E*,*H*,*I*,*L*,*M*). We observed that *CreER* expression closely resembled the *Dlx2* expression domain. Furthermore, our *Dlx1/2-CreER* transgene is for the most part expressed transiently in interneuron precursors but excluded from the progenitor B cells lying in the embryonic VZ (Fig. 2*B*,*C*). In the adult SVZ, *Dlx2* is expressed in transit-amplifying cells (C cells) and migrating neuroblasts (A cells) (Porteus et al., 1994; Doetsch et al., 2002). To identify the initially labeled population in our fate-mapping study, we analyzed the brains after 24 h of tamoxifen administration and found that YFP+ cells were within the domain of *Dlx2* expression. Namely, we detected YFP+ cells 24 h after CreER induction in the ventral telencephalon at E13.5 (Fig. 2*C*), and the SVZ (Fig. 2*F*,*J*,*N*) and RMS at later time points (data not shown). When tamoxifen was administered at the embryonic time points E15.5, E17.5, and P0, we detected some YFP+ cells in the most internal layer of the OB (Fig. 2*G*), but not in the superficial layers of the olfactory bulb, suggesting that recombination has occurred in migrating neuroblasts in the OB at these ages. However, no green cells were detected in the OB when tamoxifen was administered between P10 and P30 (Fig. 2*K*,*O*), perhaps because of a longer period of migration in older animals. No YFP+ cells were detected in the SVZ 7 d after tamoxifen administration (data not shown), indicating that our method does not result in the labeling of B cells. This affords greater temporal control, because we are labeling only the transit-amplifying progenitor cells without marking the resident stem cell populations.

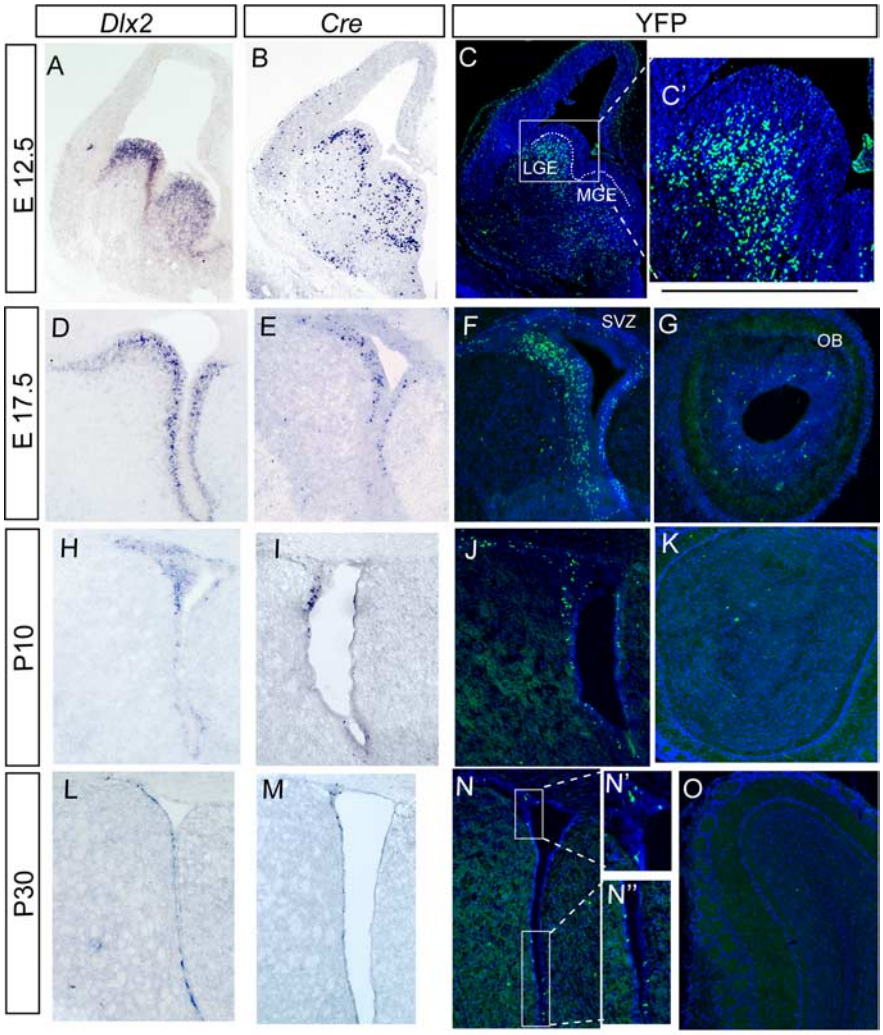

Figure 2. Short-term fate-mapping analysis. *Dlx1/2-CreER RosaYFP* animals were given tamoxifen (tx) at various time points and killed 24 h later to compare *Dlx2* expression (***A***, ***D***, ***H***, ***L***) with Cre expression (***B***, ***E***, ***I***, ***M***) and YFP expression/recombination in the LGE (***C***, ***C′***), SVZ (***F***, ***J***, ***N***, ***N′***, ***N″***), and the olfactory bulb (***G***, ***K***, ***O***). ***A–C***, E12.5 tx administration, E13.5 analysis. ***D–G***, E17.5 tx administration, E18.5 analysis. ***H–K***, P10 tx administration, P11 analysis. ***L–O***, P30 tx administration, P31 analysis. ***N′***, Dorsal SVZ YFP expression. ***N″***, Ventral SVZ YFP expression.

Analysis of OB interneuron diversity

OB interneurons are morphologically and immunohistochemically diverse (Fig. 3) (Ramon y Cajal, 1911; Price and Powell, 1970a,b,c; Pinching and Powell, 1971a,b,c). They occupy every layer of the OB and contact excitatory cells at multiple points along the pathway of olfactory information. In our studies, we were able to fate map all seven subtypes described in Figure 3. For instance, in the GL, depending on the time point of tamoxifen administration we were able to label three distinct, nonoverlapping interneuronal subtypes: TH- (Fig. 3*A*,*B*, blue), CB- (Fig. 3*A*,*B*, green), and CR (Fig. 3*A*,*C*, red)-positive interneurons. TH-positive interneurons, which possess the largest soma of the three glomerular interneuron subtypes, receive synapses from olfactory receptor neuron axons, and in turn synapse with the dendrites of mitral and tufted cells (Kosaka et al., 1998). CR- and CB-positive cells make dendritic contacts with mitral and tufted cells, and CB-positive cells also occasionally contact other interneurons (Kosaka et al., 1998). We have confirmed that the overlap in expression of three glomerular interneuron subtypes is negligible by performing double-labeling experiments in wild-type animals (data not shown).

We were also able to label a class of PV-positive interneuron (Fig. 1*A*,*E*, orange) residing primarily in the EPL. These cells are GABAergic (Kosaka and Kosaka, 2005; Parrish-Aungst et al., 2007) and extend processes along the primary dendrites and

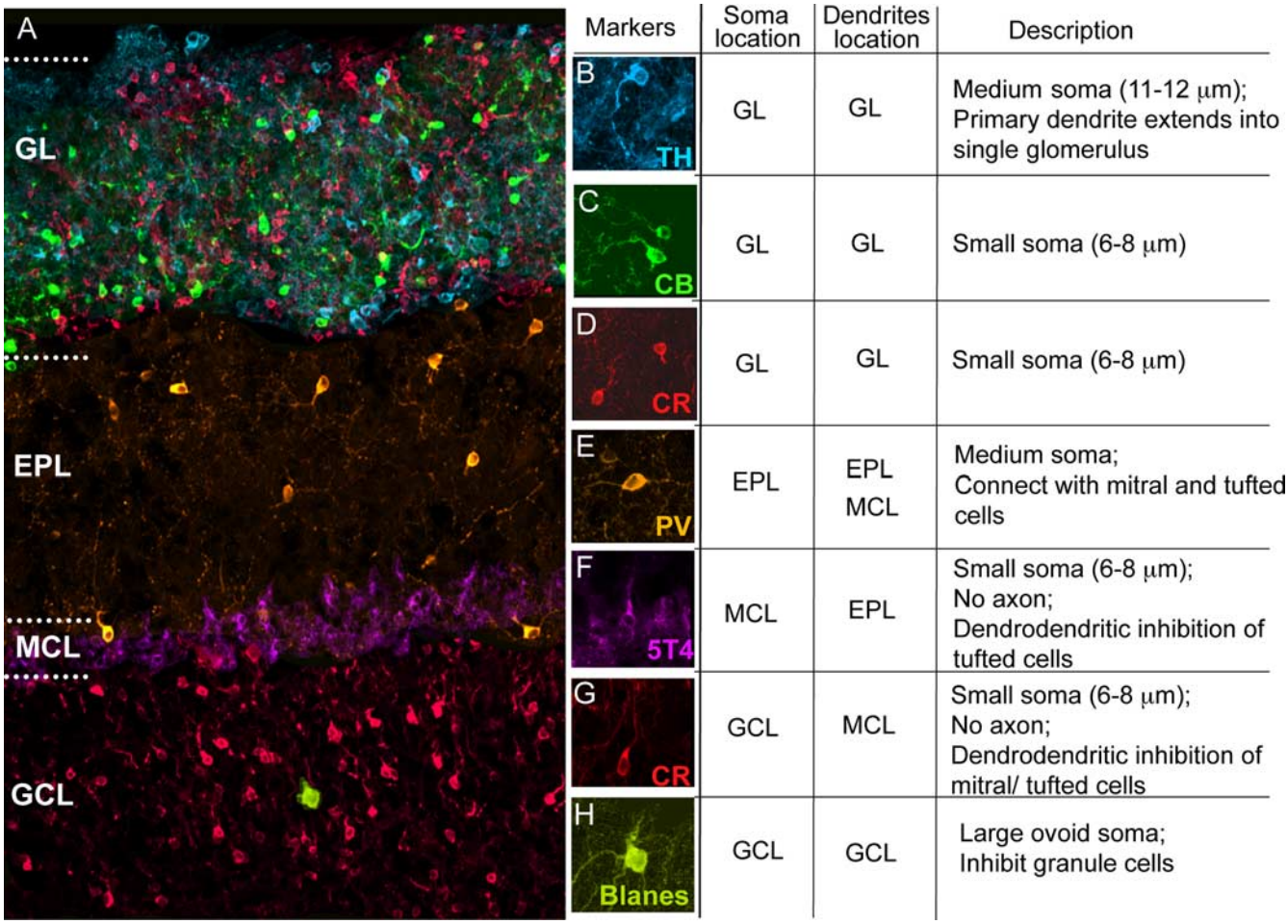

Figure 3. Olfactory bulb interneuron diversity. We could distinguish seven OB interneuron populations based on their position and expression of immunomarkers. ***A***, Example section of mouse olfactory bulb. ***B***, TH-expressing GL cell (blue). ***C***, CB-expressing GL cell (green). ***D***, CR-expressing GL cell (red). ***E***, PV-expressing EPL cell (orange). ***F***, 5T4-expressing MCL granule cell (purple). ***G***, CR-expressing GCL granule cell (red). ***H***, CB-positive Blanes cell in GCL (green).

soma of mitral and tufted cells (Kosaka et al., 1994; Toida et al., 1996; Crespo et al., 2001; Kosaka and Kosaka, 2007).

Granule cells have a small soma and no axon and establish dendrodendritic connections with excitatory neurons (Price and Powell, 1970a,b). We were able to fate map at least two classes of granule cells in the mitral cell layer (MCL) and GCL, based on their expression of 5T4 (Fig. 1*A*,*F*, purple in MCL) and CR (Fig. 1*A*,*G*, red in GCL). 5T4-positive granule cells are the most externally situated population of granule cells, and make dendrodendritic contacts with excitatory cells in the superficial EPL (Imamura et al., 2006). CR-positive granule cells were located in the external part of the GCL, and make dendrodendritic contacts with excitatory cells throughout the EPL. It should be noted, however, that many of the YFP+ granule cells we fate mapped, including all the ones in the internal GCL, did not colabel with any of the markers we used. In addition, we detect Blanes cells, which are large, ovoid interneurons with a unique morphology within the GCL (Fig. 1*A*,*H*, green in GCL) (Blanes, 1898; Schneider and Macrides, 1978; Pressler and Strowbridge, 2006). Blanes cells are GABAergic persistent spiking interneurons that inhibit granule cells (Pressler and Strowbridge, 2006), therefore regulating the strength of inhibition of tufted and mitral cell activity. Because of their persistent spiking properties, it has been suggested that these cells are involved in short-term olfactory memory via lasting modulation of local circuit activity (Pressler and Strowbridge, 2006). All of the subtypes of interneurons we identified have previously been reported to be GABAergic (Parrish-Aungst et al., 2007). Most of our analysis was performed on P30 animals; however, we compared P30, P45, and P60 OBs for marker expression and saw no significant difference in the interneuron distribution across those ages (data not shown).

Glomerular interneuron production declines with age

Using the tamoxifen administration time points outlined in Figure 1, we performed immunohistochemistry on OB sections from fate-mapped *Dlx1/2-CreER RosaYFP* animals to analyze the distribution patterns of OB interneuron production for each time point. We find that YFP+ cells are present in the OB of animals given tamoxifen between E12.5 and P30. When the number of YFP+ cells/mm^2 is quantified, we find that animals in which tamoxifen is administered between P0 and P10 contain the highest number of YFP+ cells per area (Fig. 4*A*). This is in agreement with tritiated thymidine birthdating studies performed in rats showing that the majority of OB interneurons are produced perinatally (Bayer, 1983). Furthermore, in accordance with these birthdating studies, we observe a temporal shift in the layer destination of cells fate mapped from the *Dlx1/2* lineage. Specifically, a higher percentage of the total YFP+ population is located in the

glomerular layer in animals fate mapped from E12.5 and E15.5 than in animals fate mapped from late-embryonic and postnatal ages (Fig. 4*A*). This is accompanied by a concomitant increase in the percentage of YFP+ cells destined for the GCL at these later ages. We did not observe any YFP+ excitatory neurons or glial cells at any time point, as assessed by the morphology of the cells as well as expression of Tbrain1, Reelin, PDGFRα, or GFAP (data not shown). Together, these results show that the *Dlx1/2*-expressing progenitor population contributes interneurons to the OB throughout the life of the animal, with peak production occurring early postnatally. In addition, glomerular interneurons appear to be born preferentially at the earliest time points.

To assess whether a significant degree of cell death occurs within our fate-mapped populations, we examined the expression of cleaved caspase-3 in the olfactory bulbs at all the time points analyzed (supplemental Fig. 1, available at www.jneurosci.org as supplemental material). The percentage of the fate-mapped cells undergoing cell death (i.e., caspase-3+/YFP+ cells) were so few that it is difficult to imagine they impact the percentages of different subtypes that we observe. We can not, however, rule out that specific subpopulations are not significantly winnowed in number by cell death before their integration in the bulb (i.e., in the time intervening between being genetically labeled and observed at the P30 or P60 analysis time point).

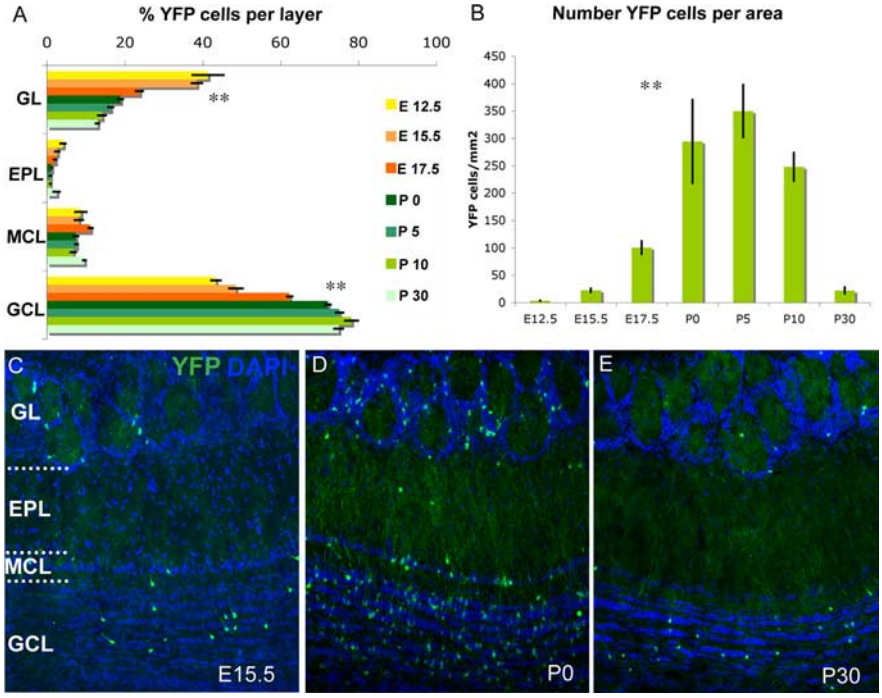

Figure 4. *Dlx1/2-CreER RosaYFP* temporal fate mapping. ***A***, The percentage of YFP+ cells residing in each layer of OB from animals fate mapped at E12.5 (yellow), E15.5 (light orange), E17.5 (dark orange), P0 (dark green), P5 (green), P10 (lime green), and P30 (light green). ***B***, The number of YFP+ cells/mm^2 of olfactory bulb. E12.5, 3.54 ± 0.3 YFP+ cells/mm^2; $n = 4$ animals. E15.5, 22.4 ± 3.5 YFP+ cells/mm^2; $n = 4$ animals. E17.5, 100 ± 12 cells/mm^2; $n = 4$ animals. P0, 294 ± 76 cells/mm^2; $n = 3$ animals. P5, 350 ± 48 cells/mm^2; $n = 3$ animals. P10, 248 ± 26 cells/mm^2; $n = 4$ animals. P30, 22 ± 6 cells/mm^2; $n = 3$ animals. ***C***, Example section from E15.5 tamoxifen administration, P30 analysis, immunostained for YFP (green) and stained with DAPI (blue) nuclear stain. ***D***, P0 tamoxifen administration, P30 analysis. ***E***, P30 tamoxifen administration, P60 analysis. Error bars represent SEM. $^{**}p < 0.0001$, ANOVA.

Glomerular interneuron subtypes are produced in distinct temporal patterns

To determine whether there is a temporal bias in the production of specific interneuron subtypes, we analyzed the immunomarkers expressed by interneurons fate mapped in *Dlx1/2-CreER RosaYFP* animals. We found that each of the three immunological subtypes (TH, CB, and CR) has a unique temporal production profile (Fig. 5*B*). TH-positive interneurons made up the largest percentage of YFP+ interneurons in the GL (60.7 ± 8%) in animals fate mapped from E12.5, the earliest time point examined (Fig. 5*B–F*). In animals fate mapped from this age, CB- and CR-positive interneurons make up only a small percentage of YFP+ GL cells (5.6 ± 3% and 2.5 ± 2%, respectively) (Fig. 5*B*,*I*,*J*). In contrast, in animals fate mapped from late embryonic ages, E15.5 and E17.7, CB-positive interneurons make up the highest percentage of YFP+ cells in the GL at 16.6 ± 1% and 16.1 ± 1%, respectively (Fig. 5*B*,*G–J*). TH+ fate-mapped interneurons decline in percentage with time, making up 14.5 ± 2% of GL fate-mapped cells at E15.5 and 8.2 ± 2% at E17.5 (Fig. 5*B*). Interestingly, P0 represents the only time point at which we observed that CB, CR, and TH glomerular neurons are produced in equivalent numbers (Fig. 5*B*). Although CR-positive interneurons constitute a relatively small percentage of embryonic fate-mapped GL, this population of interneurons increases with age and constitutes the highest percentage of GL fate-mapped cells postnatally (Fig. 5*B*,*K–N*). These data indicate that the *Dlx1/2* lineage produces unique GL interneuron subpopulations at different developmental stages.

PV-expressing interneurons are produced at early postnatal time points

To date, analysis of OB interneuron diversity has been largely confined to glomerular interneurons. Here we analyze for the first time the temporal production of PV interneurons located in the EPL. Remarkably, we did not observe any PV+/YFP+ double-labeled cells in animals administered tamoxifen at E12.5 or P30 (Fig. 6*B*), making this the only interneuron subtype that could not be fate mapped from adult ages. The highest percentage of YFP+ cells colabeling with PV occurred in animals fate mapped from P10 (29.9 ± 4%) (Fig. 6*B–F*). This demonstrates that there is a critical period for PV cell production during the first few weeks of the animal's life.

5T4 and CR+ granule cells are produced in different temporal patterns

It is likely that different subtypes of granule cells interact with different projection neurons, which in turn have different firing properties (Nagayama et al., 2004), thereby mediating a different output. To assess the temporal production of different types of fate-mapped granule cells, we analyzed both their position and expression of 5T4 or CR. The proportion of 5T4-expressing granule cells destined for the MCL appears to be constant throughout the life of the animal (Fig. 7*B*,*D–G*). In contrast, we observed that the largest percentage of GCL YFP+ cells colabeled with CR (12.8 ± 1%) occurred in animals given tamoxifen at P0 (Fig. 7*C*,*H–K*). Furthermore, the postnatal percentage of YFP+ cells

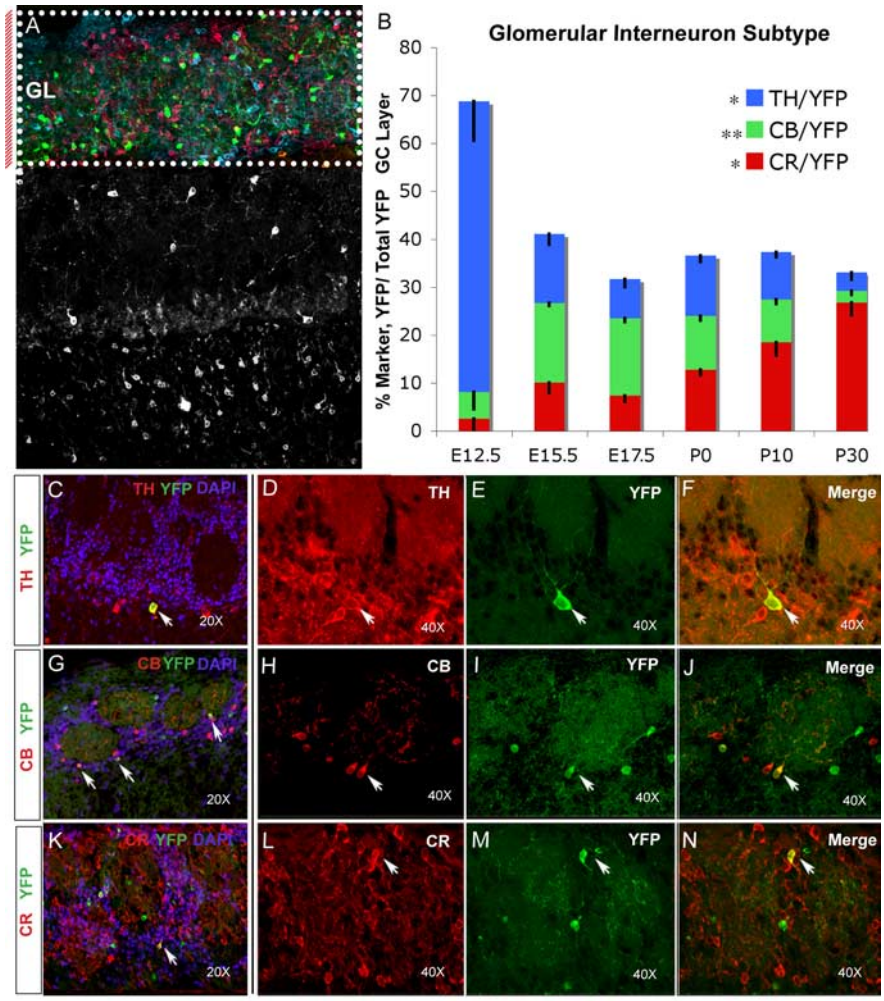

Figure 5. Temporal fate mapping of GL interneurons. ***A***, Boxed colored micrograph with red bar to left indicates that this analysis is confined to the GL. ***B***, A percentage comparison of the relative production of TH, CB, and CR interneuron subtypes produced at different time points during development. At E12.5, TH-positive cells (blue bars) make up the largest percentage (60.7 ± 8), followed by CB (green bars; 5.6 ± 4) and CR (red bars; 2.5 ± 2); at E15.5, CB-positive cells make up the highest percentage at 16.6 ± 1, followed by TH (14.5 ± 2) and CR (10.1 ± 2); at E17.5, CB-positive cells make up the highest percentage at 16.1 ± 1, followed by TH (8.2 ± 2) and CR (7.3 ± 1); at P0, all three subtypes are produced in similar proportions: TH, 12.6 ± 1; CB, 11.2 ± 1; and CR, 12.7 ± 1; at P10, CR-positive cells make up the majority of GL cells at 18.5 ± 2, followed by TH (9.9 ± 1) and CB (8.9 ± 1); finally, at P30, CR-positive cells make up 26.8 ± 3% of GL YFP+ cells, followed by TH (3.9 ± 2) and CB (2.4 ± 1). Error bars indicate SEM. *$p < 0.005$, ANOVA; **$p < 0.0001$, ANOVA. ***C***, Example 20× section from E12.5 fate-mapped OB GL, showing TH (red), YFP (green), and DAPI (blue); arrow indicates double-labeled cell. ***D–F***, Example 40× section from E12.5 fate-mapped OB GL; shown are TH (***D***, red), YFP (***E***, green), and merge (***F***); arrows indicate TH/YFP double-positive cell. ***G***, Example 20× section from E17.5 fate-mapped OB GL; shown are CB (red), YFP (green), and DAPI (blue); arrows indicate double-labeled cells. ***H–J***, Example 40× section from E17.5 fate-mapped OB GL; shown are CB (***H***, red), YFP (***I***, green), and merged image (***J***); arrows indicate CB/YFP double-labeled cell. ***K***, Example 20× section from P0 fate-mapped OB GL; shown are CR (red), YFP (green), and DAPI (blue); arrow indicates double-labeled cell. ***L–N***, Example 40× section from P0 fate-mapped OB GL; shown are CR (***L***, red), YFP (***M***, green), and merged image (***N***); arrows indicate CR/YFP double-labeled cell.

expressing CR in the GCL was higher than at embryonic ages (Fig. 7*C*). This suggests that, similar to CR-positive GL interneurons, extrinsic or intrinsic factors present after birth favor the production of CR-positive granule cells over other granule cell subtypes. In accordance with what has been previously described, we observe that granule cells are the predominant interneuron type generated in the adult (Betarbet et al., 1996; Luskin, 1998). In summary, our data show that different OB interneuron subtypes that interact with different output neurons are preferentially produced in different patterns.

Blanes cells are predominantly produced embryonically

Contrary to granule cells, Blanes cells appear to be preferentially generated before birth. Indeed, they are produced in their greatest abundance in animals fate mapped from E12.5 and E15.5, at 1.4 ± 0.5% and 1.5 ± 0.5%, respectively (Fig. 8*B–F*). A subset of Blanes cells was observed to express CB in these studies (Fig. 8*C–E*).

Discussion

In this study we observed that at least seven subtypes of OB interneurons are derived from the *Dlx1/2*-expressing precursor domain. We also find that each of these subtypes is produced in a unique temporal pattern (Fig. 9). For instance, embryonic *Dlx1/2* precursors destined for the GL are more likely to give rise to TH- (Fig. 9*A*) or CB-expressing interneurons (Fig. 9*B*) than their postnatal counterparts, which predominantly differentiate into CR-expressing GL interneurons (Fig. 9*C*). We also show that PV-expressing cells destined for the EPL are derived from the *Dlx1/2* lineage and are produced only from late embryogenesis through the first few weeks of life, but not in the adult (Fig. 9*D*). We demonstrate that 5T4-expressing granule cells are generated at approximately the same proportion at all the time points fate mapped (Fig. 9*E*), whereas the CR-positive granule cell population reaches a peak early postnatally (Fig. 9*F*). In addition, we find that Blanes cells, although produced at all the time points examined, make up the greatest percentage of GCL YFP+ cells when animals are fate mapped at embryonic ages (Fig. 9*G*). Our findings extend the recent observation that specific OB interneuron subtypes arise from distinct spatial locations by demonstrating that each of these discrete niches produce specific interneuron populations with a unique temporal profile.

We find that our fate-mapping results differ significantly from previous attempts to characterize the temporal specificity of OB interneuron subtype production. For instance, using fluorogold labeling techniques, De Marchis et al. (2007) found that very few neonatally labeled progenitors become TH+ interneurons. Specifically, they report that TH+ cells are derived predominantly from cells labeled in adult animals. In contrast, we find that a sizeable portion of neonatal *Dlx1/2* progenitors become TH+ cells, whereas very few cells derived from the adult Dlx1/2 lineage do so. In fact we find that at E12.5, TH+ cells comprise the majority of those found in the GL. De Marchis et al. (2007) confined their study to postnatal times. It is, therefore, somewhat difficult to extrapolate their work to embryonic ages. However, their results using dye-

labeling techniques appear to suggest exactly the opposite trend in the product of TH+ neurons from what we observed using genetic fate mapping. Whereas their results suggest that the production of TH+ cells within the GL interneuron increases at later postnatal time points, we find that TH+ cell production is greatest at embryonic time points and thereafter declines precipitously.

The dye labeling experiments in the De Marchis et al. (2007) study are not only inconsistent with our observations, they appear to contradict the findings of the homochronic transplant experiments performed by the authors themselves. For instance, they observe that 20% of the labeled cells within the GL expressed CB after neonatal dye injections. However, only 5% of the homochronically transplanted GL cells in this same study were found to be CB positive. This inconsistency could be explained in a number of ways. Most probably, the authors were inadvertently examining distinct progenitor populations in their transplant and dye-labeling studies. Alternatively, transplant techniques may have an adverse affect on specific progenitor subtypes depending on the age of the animal used for progenitor donation or cause selective damage of one or more progenitor niches present in the host animal. Regardless of the specific underlying cause, the recent recognition that different OB interneuronal subtypes arise from multiple, spatially discreet progenitor domains (Merkle et al., 2007) makes comprehensive analysis using dye labeling or transplant studies of temporal OB interneuron production difficult, if not impossible.

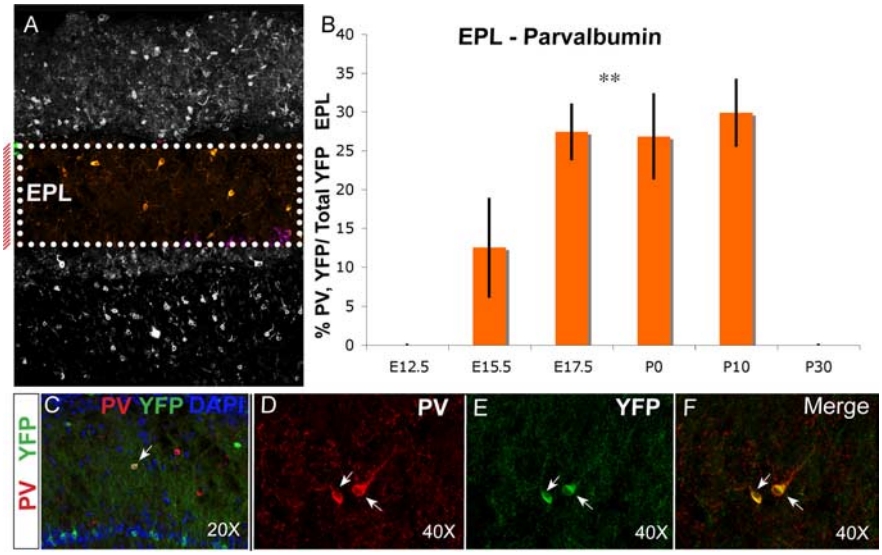

Figure 6. Production of PV cells of the EPL over time. ***A***, Boxed colored micrograph with red bar to left indicates that this analysis is confined to the EPL. ***B***, Quantification of percentage of EPL YFP+ cells expressing PV from each fate-mapped time point. Of cells from E12.5 and P30 animals in EPL, 0% were PV+; at E15.5, 12.5 ± 6% of EPL YFP+ cells expressed PV; at E17.5, 27.4 ± 4% expressed PV; at P0, 26.8 ± 5% expressed PV; and at P10, 29.9 ± 4% were PV positive. $^{**}p < 0.001$, ANOVA. ***C***, Example 20× section of EPL from P10 fate-mapped animal showing PV (red), YFP (green), and DAPI (blue). Arrow indicates double-positive cell. ***D–F***, Example 40× section from P10 fate-mapped OB; shown are PV (***D***, red), YFP (***E***, green), and merge (***F***); arrows indicate double-labeled cells.

One might reasonably argue that the genetic fate-mapping approach we have used suffers from similar biases to dye or transplant studies. Although it is difficult to entirely rule this out, a number of observations suggest our approach is both more reliable and comprehensive. First, all newborn OB interneurons appear to both express and require *Dlx1* and/or *Dlx2* for their production. Second, we have been successful in labeling OB interneurons in every layer of the bulb and have identified in our fate mapping all major interneuron subclasses that have been reported previously. Third, our method is noninvasive, and the pattern of labeling corresponds well to the general outside-in trend in labeling observed in bromodeoxyuridine (BrdU) studies. Together, our study appears to provide a comprehensive sampling of OB interneurons collectively produced from each of the distinct niches at each of the time points examined.

There are multiple studies that address the role of selective cell loss in shaping the OB interneuron circuitry (Biebl et al., 2000; Petreanu and Alvarez-Buylla, 2002; Winner et al., 2002; Lemasson et al., 2005; Magavi et al., 2005; Kohwi et al., 2007; Whitman and Greer, 2007). For instance, previous studies show that superficial granule cells produced in the first few weeks of life are a stable population (Lemasson et al., 2005), whereas 50% of adult-born granule cells die within the first few months of being generated (Biebl et al., 2000; Petreanu and Alvarez-Buylla, 2002; Winner et al., 2002). It is not known whether the granule cells lost belong disproportionately to any given subtype. Furthermore, little is known about the turnover of embryonic and perinatally derived GL interneurons, but BrdU labeling studies of adult-derived glomerular interneurons suggest that CR- and TH-expressing interneurons could be lost at higher rates than CB-positive interneurons (Kohwi et al., 2007). Given that the relative proportions of glomerular cells expressing TH, CB, and CR are stable throughout life (Kohwi et al., 2007), and the pattern of apoptotic cells observed at the postnatal ages investigated is temporally static and spatially uniform (Lemasson et al., 2005), it would appear that the composition of interneurons in the olfactory bulb at any given time must be determined by a combination of temporally distinct subtype production and cell death. Although our present study addresses the initial production of interneurons, our methods could be very useful for addressing whether selective death shapes the proportion of specific interneuron subpopulations over time.

Contrary to the previous assumption that OB interneurons were entirely subpallially derived, recent studies have indicated that OB interneurons can also come from *Emx1*+ pallial domains (Kohwi et al., 2007). Despite this, we can account for most, if not all, of the known diversity of OB interneurons using the *Dlx1/2* lineage. It will be important to determine whether the dorsally derived populations represent an as yet unclassified interneuron population separate from the *Dlx1/2*-derived domain or whether *Emx1* domain-derived OB interneurons are contained within the *Dlx1/2* population. The latter possibility is suggested by the observation that *Emx1/Dlx2* double-positive progenitors have been observed (Kohwi et al., 2007). Although it is beyond the scope of the present study, we have developed an intersectional fate-mapping allele in which GFP is conditionally expressed in cells that at some point during development express both the Flpe and Cre recombinases. To this end, we are currently examining $Emx1^{Cre};Dlx5/6^{Flp}$ mice carrying this reporter allele (our unpublished results).

It will also be important to reconcile our findings with the observation that different OB interneurons appear to arise from

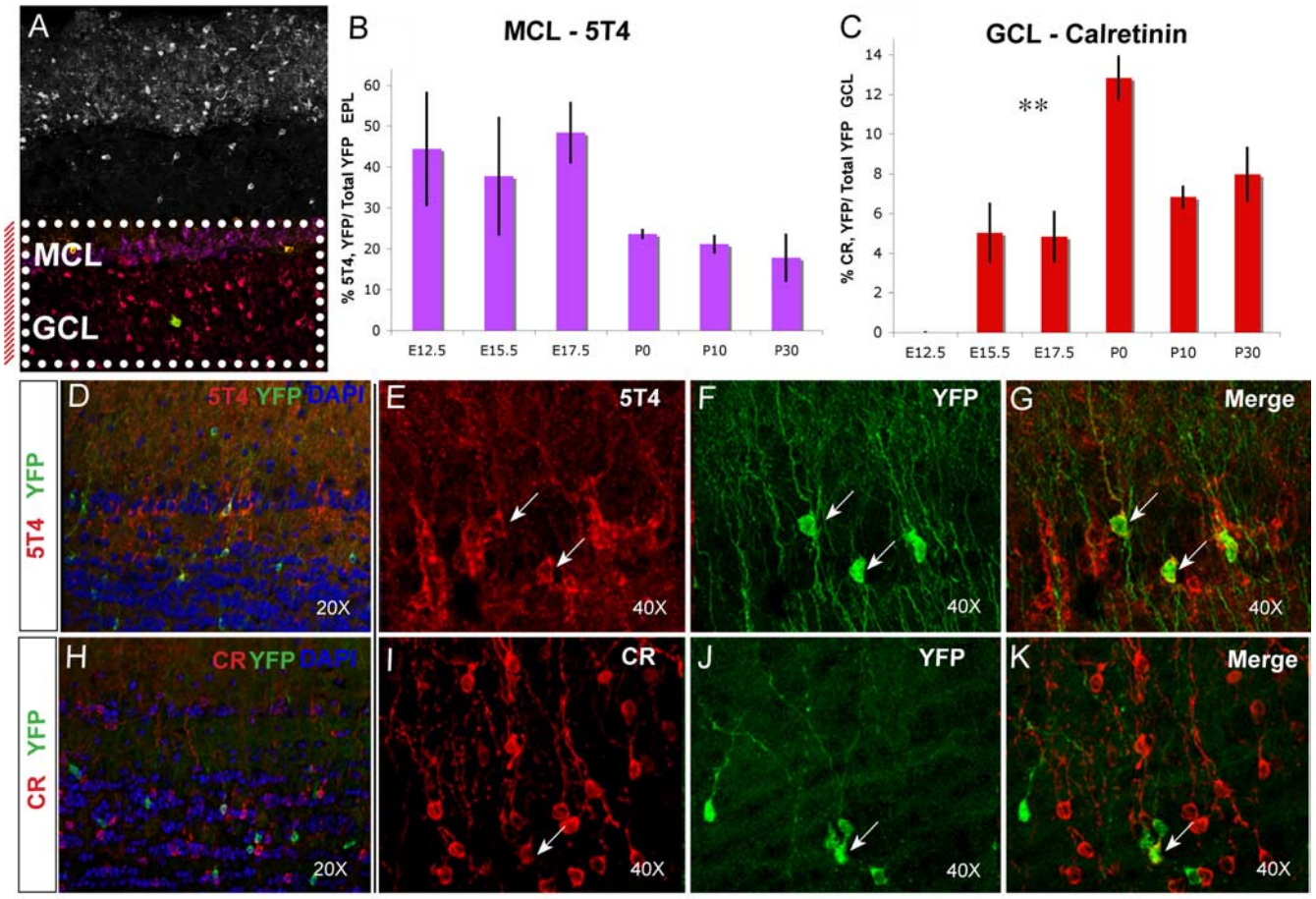

Figure 7. Temporal fate mapping of granule cell subtypes. ***A***, Boxed colored micrograph with red bar to left indicates that this analysis is confined to the MCL and GCL. ***B***, Quantification of the percentage of YFP+ cells in the MCL expressing 5T4: E12.5, 44.4 ± 13.7%; E15.5, 37.8 ± 14.2%; E17.5, 48.4 ± 7.2%; P0, 23.6 ± 1%; P10, 21.1 ± 2%; P30, 17.8 ± 6%. ***C***, Quantification of the percentage of YFP+ cells in the GCL expressing CR: E12.5, 0%; E15.5, 5 ± 1%; E17.5, 4.8 ± 1%; P0, 12.8 ± 1%; P10, 6.8 ± 1%; P30, 8.0 ± 1%. ***D***, Example 20× MCL section from E17.5 fate-mapped OB with 5T4 (red), YFP (green), and DAPI (blue) staining. ***E–G***, Example 40× section from E17.5 fate-mapped MCL granule cells expressing 5T4 (***E***, red), YFP (***F***, green), and merge (***G***); arrows indicate double-labeled cells. ***H***, Example 20× GCL section from P0 fate-mapped OB with CR (red), YFP (green), and DAPI (blue) staining. ***H–K***, Example 40× section from P0 fate-mapped GCL cells expressing CR (***H***, red), YFP (***J***, green), and merge (***K***); arrows indicate double-labeled cell. $^{**}p < 0.001$, ANOVA.

distinct stem cell progenitor populations. For instance, Merkle et al. (2007) have demonstrated by viral injection into carefully controlled spatial domains of the P0 mouse that the dorsal SVZ is more likely to give rise to TH+ GL interneurons, anteromedial domains tend to generate CR+ interneurons, and ventral progenitor pools give rise to CB+ interneurons. Notably, although we have been able to fate map all of these domains using the *Dlx1/2-CreER* animal, we observe different temporal patterns of production for each subtype. In this regard, the use of the P0 time point by the Merkle et al. (2007) study appears in retrospect to have been a particularly fortuitous choice, because this is the only period during development when all OB interneuron subtypes are simultaneously being generated.

Following the idea that OB interneurons are produced from spatially defined stem cell niches, our finding that TH+ cells are the predominant cell type produced at early embryonic ages suggests that the dorsal niche could be one of the earliest to begin OB interneuron production. Likewise, our finding that the CR+ cells are the predominant cell type produced at later ages suggests the anteromedial niche is most active postnatally. It will be interesting to determine whether and why progenitor domains might come to dominate in their production of OB interneurons during specific time windows. This is especially true given that the most diversity is generated around the birth of the animal, and hence the beginning of olfactory sensory activity. We find that CR and PV+ cell production dominates at this time point. It is therefore tempting to speculate that these interneuron subtypes are produced during an olfactory critical period. If this is true, their production and/or morphology could be heavily influenced by the activity of their neighboring cells.

These speculations aside, our findings are significant in that, although previous BrdU and tritiated thymidine birthdating studies have shown changes in the numbers and positions of cells destined for the bulb, these studies did not investigate the specific immunological subtypes produced. Furthermore, genetic fate mapping allows us to investigate morphological differences in interneuron subtypes produced at specific time points. For instance, using classical birthdating techniques it would be impossible to determine whether a GCL cell were a granule cell or Blanes cell. Because we have demonstrated that it is possible to selectively mark specific, temporally derived populations with the *Dlx1/2-CreER* line, future studies can investigate the physiology of these interneuron subtypes. In particular it will be interesting to study the effects of environmental cues, such as activity, on the morphological characteristics of these cells, such as dendrite location, spine density, and soma size.

References

Alvarez-Buylla A, Garcia-Verdugo JM (2002) Neurogenesis in adult subventricular zone. J Neurosci 22:629–634.

Anderson SA, Qiu M, Bulfone A, Eisenstat DD, Meneses J, Pedersen R, Rubenstein JL (1997) Mutations of the homeobox genes Dlx-1 and Dlx-2 disrupt the striatal subventricular zone and differentiation of late born striatal neurons. Neuron 19:27–37.

Aungst JL, Heyward PM, Puche AC, Karnup SV, Hayar A, Szabo G, Shipley MT (2003) Centre-surround inhibition among olfactory bulb glomeruli. Nature 426:623–629.

Bayer SA (1983) 3H-thymidine-radiographic studies of neurogenesis in the rat olfactory bulb. Exp Brain Res 50:329–340.

Betarbet R, Zigova T, Bakay RA, Luskin MB (1996) Dopaminergic and GABAergic interneurons of the olfactory bulb are derived from the neonatal subventricular zone. Int J Dev Neurosci 14:921–930.

Biebl M, Cooper CM, Winkler J, Kuhn HG (2000) Analysis of neurogenesis and programmed cell death reveals a self-renewing capacity in the adult rat brain. Neurosci Lett 291:17–20.

Blanes T (1898) Sobre algunos puntos dudosos de la estructura del bulbo olfactorio. Rev Trimest Microgr 3:99–127.

Bulfone A, Kim HJ, Puelles L, Porteus MH, Grippo JF, Rubenstein JL (1993) The mouse Dlx-2 (Tes-1) gene is expressed in spatially restricted domains of the forebrain, face and limbs in midgestation mouse embryos. Mech Dev 40:129–140.

Bulfone A, Wang F, Hevner R, Anderson S, Cutforth T, Chen S, Meneses J, Pedersen R, Axel R, Rubenstein JL (1998) An olfactory sensory map develops in the absence of normal projection neurons or GABAergic interneurons. Neuron 21:1273–1282.

Crespo C, Blasco-Ibanez JM, Marques-Mari AI, Martinez-Guijarro FJ (2001) Parvalbumin-containing interneurons do not innervate granule cells in the olfactory bulb. NeuroReport 12:2553–2556.

De Marchis SBS, Carletti B, Hsieh YC, Garzotto D, Peretto P, Fasolo A, Puche AC, Rossi F (2007) Generation of distinct types of periglomerular olfactory bulb interneurons during development and in adult mice: implication for intrinsic properties of the subventricular zone progenitor population. J Neurosci 27:657–664.

Doetsch F, Garcia-Verdugo JM, Alvarez-Buylla A (1997) Cellular composition and three-dimensional organization of the subventricular germinal zone in the adult mammalian brain. J Neurosci 17:5046–5061.

Doetsch F, Caille I, Lim DA, Garcia-Verdugo JM, Alvarez-Buylla A (1999) Subventricular zone astrocytes are neural stem cells in the adult mammalian brain. Cell 97:703–716.

Doetsch F, Petreanu L, Caille I, Garcia-Verdugo JM, Alvarez-Buylla A (2002) EGF converts transit-amplifying neurogenic precursors in the adult brain into multipotent stem cells. Neuron 36:1021–1034.

Feil R, Wagner J, Metzger D, Chambon P (1997) Regulation of Cre recombinase activity by mutated estrogen receptor ligand-binding domains. Biochem Biophys Res Commun 237:752–757.

Firestein S (2001) How the olfactory system makes sense of scents. Nature 413:211–218.

Ghanem N, Yu M, Long J, Hatch G, Rubenstein JL, Ekker M (2007) Distinct cis-regulatory elements from the Dlx1/Dlx2 locus mark different progenitor cell populations in the ganglionic eminences and different subtypes of adult cortical interneurons. J Neurosci 27:5012–5022.

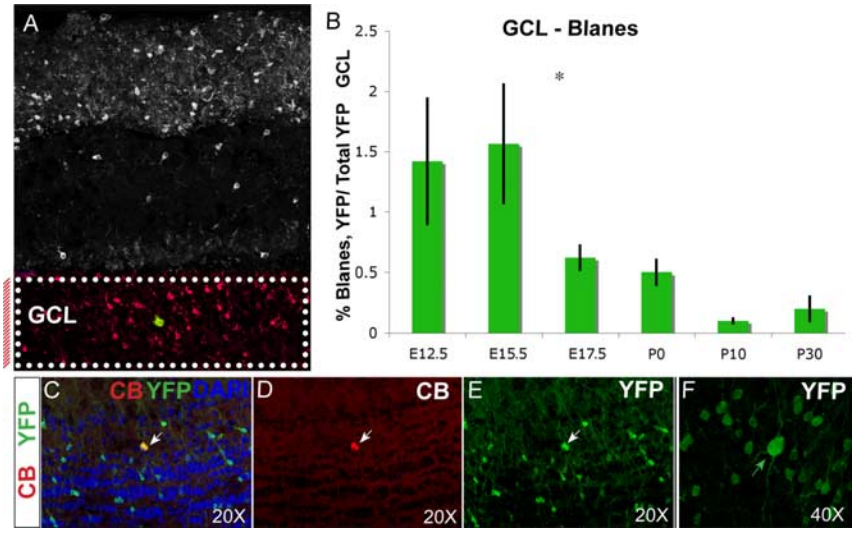

Figure 8. Blanes cell fate mapping. ***A***, Boxed colored micrograph with red bar to left indicates that this analysis is confined to the GCL. ***B***, Quantification of Blanes cell production as a percentage of YFP+ cells in the GCL: E12.5, 1.4 ± 0.5%; E15.5, 1.6 ± 0.5%; E17.5, 0.6 ± 0.1%; P0, 0.5 ± 0.1%; P10, 0.1 ± 0.02%; P30, 0.2 ± 0.1%. ***C–E***, Example 20× GCL section from an E17.5 fate-mapped animal (***C***, merge) showing a CB-positive (***D***, red) Blanes cell, double positive for YFP (***E***, green); arrows indicate double-positive cell. ***F***, Example 40× section from P0 fate-mapped animal showing YFP-positive (green) Blanes cell in the GCL. *$p < 0.05$, ANOVA.

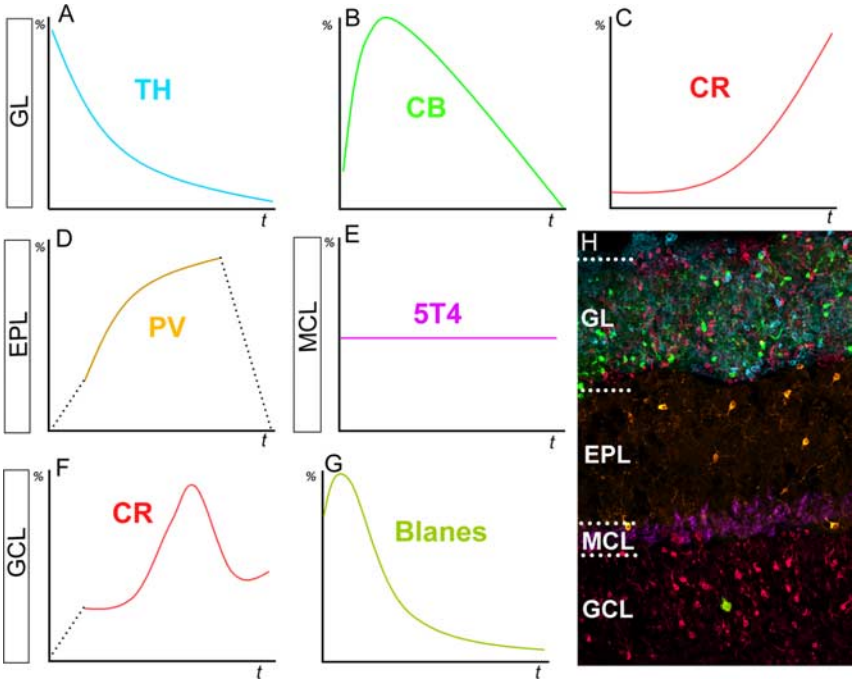

Figure 9. Summary of temporal patterns of OB interneuron production. ***A***, TH+ GL cells make up the highest percentage of YFP+ cells during early embryogenesis and decline with the age of the animal as a percentage of GL cells produced. ***B***, CB+ cells make up the highest percentage of YFP+ GL cells during late embryogenesis and decline thereafter. ***C***, CR+ GL cells make up a very small percentage of YFP+ cells during embryogenesis, but increase with the age of the animal fate mapped. ***D***, PV+ cells are not produced at E12.5 or P30, but make up a substantial proportion of EPL YFP+ cells fate mapped from late embryogenesis and early postnatal ages. ***E***, 5T4-positive granule cell production does not change significantly with the age of the fate-mapped animal. ***F***, CR-positive granule cell production reaches a peak as a percentage of YFP+ GCL cells just after birth. ***G***, Blanes cells make up the highest percentage of GCL cells during embryonic ages. ***H***, Interneurons of the OB: TH (blue), CB (green), CR (red), PV (orange), and 5T4 (purple).

Gorski JA, Talley T, Qiu M, Puelles L, Rubenstein JL, Jones KR (2002) Cortical excitatory neurons and glia, but not GABAergic neurons, are produced in the Emx1-expressing lineage. J Neurosci 22:6309–6314.

Hack MA, Saghatelyan A, de Chevigny A, Pfeifer A, Ashery-Padan R, Lledo PM, Gotz M (2005) Neuronal fate determinants of adult olfactory bulb neurogenesis. Nat Neurosci 8:865–872.

Hinds JW (1968a) Autoradiographic study of histogenesis in the mouse olfactory bulb. I. Time of origin of neurons and neuroglia. J Comp Neurol 134:287–304.

Hinds JW (1968b) Autoradiographic study of histogenesis in the mouse olfactory bulb. II. Cell proliferation and migration. J Comp Neurol 134:305–322.

Imamura F, Nagao H, Naritsuka H, Murata Y, Taniguchi H, Mori K (2006) A leucine-rich repeat membrane protein, 5T4, is expressed by a subtype of granule cells with dendritic arbors in specific strata of the mouse olfactory bulb. J Comp Neurol 495:754–768.

Kohwi M, Petryniak MA, Long JE, Ekker M, Obata K, Yanagawa Y, Rubenstein JL, Alvarez-Buylla A (2007) A subpopulation of olfactory bulb GABAergic interneurons is derived from Emx1- and Dlx5/6-expressing progenitors. J Neurosci 27:6878–6891.

Kosaka K, Kosaka T (2005) synaptic organization of the glomerulus in the main olfactory bulb: compartments of the glomerulus and heterogeneity of the periglomerular cells. Anat Sci Int 80:80–90.

Kosaka K, Kosaka T (2007) Chemical properties of type 1 and type 2 periglomerular cells in the mouse olfactory bulb are different from those in the rat olfactory bulb. Brain Res 1167:42–55.

Kosaka K, Heizmann CW, Kosaka T (1994) Calcium-binding protein parvalbumin-immunoreactive neurons in the rat olfactory bulb. 2. Postnatal development. Exp Brain Res 99:205–213.

Kosaka K, Toida K, Aika Y, Kosaka T (1998) How simple is the organization of the olfactory glomerulus?: the heterogeneity of so-called periglomerular cells. Neurosci Res 30:101–110.

Lemasson M, Saghatelyan A, Olivo-Marin JC, Lledo PM (2005) Neonatal and adult neurogenesis provide two distinct populations of newborn neurons to the mouse olfactory bulb. J Neurosci 25:6816–6825.

Lledo PM, Gheusi G, Vincent JD (2005) Information processing in the mammalian olfactory system. Physiol Rev 85:281–317.

Long JE, Garel S, Alvarez-Dolado M, Yoshikawa K, Osumi N, Alvarez-Buylla A, Rubenstein JL (2007) Dlx-dependent and -independent regulation of olfactory bulb interneuron differentiation. J Neurosci 27:3230–3243.

Luskin MB (1993) Restricted proliferation and migration of postnatally generated neurons derived from the forebrain subventricular zone. Neuron 11:173–189.

Luskin MB (1998) Neuroblasts of the postnatal mammalian forebrain: their phenotype and fate. J Neurobiol 36:221–233.

Luskin MB, Boone MS (1994) Rate and pattern of migration of lineally-related olfactory bulb interneurons generated postnatally in the subventricular zone of the rat. Chem Senses 19:695–714.

Magavi SS, Mitchell BD, Szentirmai O, Carter BS, Macklis JD (2005) Adult-born and preexisting olfactory granule neurons undergo distinct experience-dependent modifications of their olfactory responses *in vivo*. J Neurosci 25:10729–10739.

McQuiston AR, Katz LC (2001) Electrophysiology of interneurons in the glomerular layer of the rat olfactory bulb. J Neurophysiol 86:1899–1907.

Merkle FT, Mirzadeh Z, Alvarez-Buylla A (2007) Mosaic organization of neural stem cells in the adult brain. Science 317:381–384.

Nagayama S, Takahashi YK, Yoshihara Y, Mori K (2004) Mitral and tufted cells differ in the decoding manner of odor maps in the rat olfactory bulb. J Neurophysiol 91:2532–2540.

Nagy A, Perrimon N, Sandmeyer S, Plasterk R (2003) Tailoring the genome: the power of genetic approaches. Nat Genet 33 [Suppl]:276–284.

Parrish-Aungst S, Shipley MT, Erdelyi F, Szabo G, Puche AC (2007) Quantitative analysis of neuronal diversity in the mouse olfactory bulb. J Comp Neurol 501:825–836.

Petreanu L, Alvarez-Buylla A (2002) Maturation and death of adult-born olfactory bulb granule neurons: role of olfaction. J Neurosci 22:6106–6113.

Pinching AJ, Powell TP (1971a) The neuron types of the glomerular layer of the olfactory bulb. J Cell Sci 9:305–345.

Pinching AJ, Powell TP (1971b) The neuropil of the glomeruli of the olfactory bulb. J Cell Sci 9:347–377.

Pinching AJ, Powell TP (1971c) The neuropil of the periglomerular region of the olfactory bulb. J Cell Sci 9:379–409.

Porteus MH, Bulfone A, Liu JK, Puelles L, Lo LC, Rubenstein JL (1994) DLX-2, MASH-1, and MAP-2 expression and bromodeoxyuridine incorporation define molecularly distinct cell populations in the embryonic mouse forebrain. J Neurosci 14:6370–6383.

Pressler RT, Strowbridge BW (2006) Blanes cells mediate persistent feedforward inhibition onto granule cells in the olfactory bulb. Neuron 49:889–904.

Price JL, Powell TP (1970a) The morphology of the granule cells of the olfactory bulb. J Cell Sci 7:91–123.

Price JL, Powell TP (1970b) The synaptology of the granule cells of the olfactory bulb. J Cell Sci 7:125–155.

Price JL, Powell TP (1970c) The mitral and short axon cells of the olfactory bulb. J Cell Sci 7:631–651.

Ramon y Cajal S (1911) Histologie du systeme nerveux de l'homme et des vertebres. Paris: Maloine.

Schneider SP, Macrides F (1978) Laminar distributions of internuerons in the main olfactory bulb of the adult hamster. Brain Res Bull 3:73–82.

Shipley MT, Ennis M (1996) Functional organization of olfactory system. J Neurobiol 30:123–176.

Srinivas S, Watanabe T, Lin CS, William CM, Tanabe Y, Jessell TM, Costantini F (2001) Cre reporter strains produced by targeted insertion of EYFP and ECFP into the ROSA26 locus. BMC Dev Biol 1:4.

Stenman J, Toresson H, Campbell K (2003) Identification of two distinct progenitor populations in the lateral ganglionic eminence: implications for striatal and olfactory bulb neurogenesis. J Neurosci 23:167–174.

Toida K, Kosaka K, Heizmann CW, Kosaka T (1996) Electron microscopic serial-sectioning/reconstruction study of parvalbumin-containing neurons in the external plexiform layer of the rat olfactory bulb. Neuroscience 72:449–466.

Toresson H, Campbell K (2001) A role for Gsh1 in the developing striatum and olfactory bulb of Gsh2 mutant mice. Development 128:4769–4780.

Tucker ES, Polleux F, LaMantia AS (2006) Position and time specify the migration of a pioneering population of olfactory bulb interneurons. Dev Biol 297:387–401.

Ventura RE, Goldman JE (2007) Dorsal radial glia generate olfactory bulb interneurons in the postnatal murine brain. J Neurosci 27:4297–4302.

Whitman MC, Greer CA (2007) Adult-generated neurons exhibit diverse developmental fates. Dev Neurobiol 67:1079–1093.

Wichterle H, Turnbull DH, Nery S, Fishell G, Alvarez-Buylla A (2001) In utero fate mapping reveals distinct migratory pathways and fates of neurons born in the mammalian basal forebrain. Development 128:3759–3771.

Wilkinson DG, Nieto MA (1993) Detection of messenger RNA by in situ hybridization to tissue sections and whole mounts. Methods Enzymol 225:361–373.

Willaime-Morawek SSR, Batista C, Labbe E, Attisano L, Gorski JA, Jones KR, Kam A, Morshead CM, van der Kooy D (2006) Embryonic cortical neural stem cells migrate ventrally and persist as postnatal striatal stem cells. J Cell Biol 175:159–168.

Winner B, Cooper-Kuhn CM, Aigner R, Winkler J, Kuhn HG (2002) Long-term survival and cell death of newly generated neurons in the adult rat olfactory bulb. Eur J Neurosci 16:1681–1689.

Zambrowicz BP, Imamoto A, Fiering S, Herzenberg LA, Kerr WG, Soriano P (1997) Disruption of overlapping transcripts in the ROSA beta geo 26 gene trap strain leads to widespread expression of beta-galactosidase in mouse embryos and hematopoietic cells. Proc Natl Acad Sci USA 94: 3789–3794.